

**Current inversions induced by resonant coupling to surface waves in a nanosized water pump**Xiaoyan Zhou,<sup>1,2</sup> Fengmin Wu,<sup>1,2,\*</sup> Yang Liu,<sup>3</sup> Jianlong Kou,<sup>2</sup> Hui Lu,<sup>4,†</sup> and Hangjun Lu<sup>2,4,‡</sup><sup>1</sup>*Department of Physics and Institute of Theoretical Physics, Shanxi University, Taiyuan 030006, China*<sup>2</sup>*Department of Physics, Zhejiang Normal University, Jinhua 321004, China*<sup>3</sup>*Department of Mechanical Engineering, The Hong Kong Polytechnic University, Hong Kong 999077, China*<sup>4</sup>*Department of Bioengineering, University of Illinois at Chicago, Chicago, Illinois 60607, USA*

(Received 18 February 2015; revised manuscript received 30 September 2015; published 24 November 2015)

We conducted a molecular dynamics simulation to investigate current inversions in a nanosized water pump based on a single-walled carbon nanotube powered by mechanical vibration. It was found that the water current depended sensitively on the frequency of mechanical vibration. Especially in the resonance region, the nanoscale pump underwent reversals of the water current. This phenomenon was attributed to the dynamics competition of the water molecules in the two sections (the left and right parts) divided by the vibrating atom and the differences in phase and decay between the two mechanical waves generated by mechanical vibration and propagating in opposite directions toward the two ends of the carbon nanotube. Our findings provide an insight into water transportation through nanosized pumps and have potential in the design of high-flux nanofluidic systems and nanoscale energy converters.

DOI: [10.1103/PhysRevE.92.053017](https://doi.org/10.1103/PhysRevE.92.053017)

PACS number(s): 47.61.-k, 05.40.-a, 05.60.Cd

**I. INTRODUCTION**

Nanosized water pumps based on carbon nanotubes (CNTs) have received attention because of their unconventional properties [1–3], which are broadly applied in a variety of fields such as desalination, energy conversion, and drug delivery [4–7]. Nanoscale systems usually have unconventional properties and behaviors that are different from those of bulk systems. Recently, both simulations and experiments have demonstrated that water molecules can enter CNTs and form novel structures confined in CNTs with appropriate radii [2,8–10]. Furthermore, water molecules can permeate through the CNTs at ultrafast rates [1–8,11,12].

Interestingly, electronic current can be generated by water transportation through single-walled carbon nanotubes (SWNTs) because of a weak coupling between water dipoles and charge carriers [13–16], suggesting that water-filled SWNTs can be used as hydroelectric power converters. Hence, if water can be pumped continuously through a CNT by mechanical vibrations from an ambient source, it will be possible to power nanoscale electrical devices by harvesting mechanical energy from ambient sources without the need for batteries. There is a strong demand for such nanosized water pumps to power nanoscale devices.

Recently, many novel concepts and blueprints for the nanoscale pump have been proposed without using an osmotic or hydrostatic pressure gradient; [17–29]. Researchers have reported that water transportation through CNTs can be driven by a chemical gradient, thermal gradient [22,28–30], electronic current [31], AC electric field [20,32], rotating electric field [18,19], electric field gradient [21], vibrating charge [33,34], or rotating charge [35]. Additionally, various mechanical methods have been proposed to pump water through CNTs. Wang and Král designed nanoscopic propellers possessing

“chemically tunable” blades that pump solvent molecules [36]. Duan and Wang used a small portion of the initially twisted wall of a CNT as an energy pump for the transportation of water molecules [27]. Conducting molecular dynamics simulations, Chang demonstrated that molecules inside a SWNT can be pumped by a domino wave [37]. A more recent study by Feng *et al.* indicated that water can be pumped by revolving a chiral CNT [17]. Guo and co-workers demonstrated by molecular dynamics simulations that an excited vibrating CNT cantilever can act as an efficient and simple nanosized water pump [38]. However, it is still difficult to pump water through a CNT continuously and controllably using only mechanical vibrations.

In our previous work, we proposed a nanosized water pump driven by an external vibrating charge [33,34,39]. Interestingly, resonance phenomena were found for these nanoscale systems, where water molecules are transported through the CNTs under the effect of external interference [34,40,41]. Furthermore, the water flux varies sharply, and sometimes reverses [33,34]. The conditions required for the emergence of directed transport are clear [42], but the question remains as to what factors affect the current inversion and the pumping capacity of the nanosized water pump. This question is an important consideration in designing a nanoscale pump.

In the present study, we employed a molecular dynamics simulation technique to demonstrate a blueprint of a nanosized water pump driven by mechanical vibration without the requirement for valves or impellers. The thermal equilibrium and spatial symmetry of the nanosized water pump are both broken by a periodic excitation at an off-center position. Pumping is achieved by mechanical waves that are created by a periodic excitation and propagate toward the two ends of an SWNT. Resonance and current inversion phenomena were observed for our nanosized water pump. The mechanism behind the complicated phenomena was investigated by analyzing the mechanical waves propagating in the SWNT. Our findings help clarify the relationship between the water flux and the vibration frequency of external stimuli and in predicting the actual direction of water transport in nanoscopic valveless pumps.

\*Corresponding author: [wfm@zjnu.cn](mailto:wfm@zjnu.cn)†Corresponding author: [huilu@uic.edu](mailto:huilu@uic.edu)‡Corresponding author: [zjlhjun@zjnu.cn](mailto:zjlhjun@zjnu.cn)

TABLE I. Simulation systems.

Scenario	SWNT	Vibrating atom	Amplitude	System name
1	(10,10), 7.15 nm long	12	0.15 nm	sys1
2	(6,6), 7.15 nm long	12	0.075 nm	sys2
3	(10,10), 14.43 nm long	23	0.15 nm	sys3

## II. SIMULATION METHODS

We prepared three systems with different types of SWNT (as listed in Table I). The first system, named sys1, is illustrated in Fig. 1. An uncapped (10,10) armchair SWNT with length of 7.15 nm and diameter of 1.35 nm is embedded in the membranes along the  $z$  direction. The carbon membrane atoms are located in a face-centered-cubic fashion in the  $xy$  plane. The membranes, together with the bottom part and two ends of the SWNT, are fixed during the simulations. A carbon atom, called the vibrating atom, on the left side of the carbon tube moves along the  $x$  axis according to the equation of motion  $x = x_0 + A\cos(\omega t + \varphi) - A$ , where  $x_0$  is the initial position of the vibrating carbon atom,  $A$  is the amplitude,  $\omega$  is the angular frequency, and  $\varphi$  is the initial phase. The frequency  $f$  is defined as  $\omega/2\pi$ . Consequently, some carbon atoms neighboring the vibrating atom move cooperatively when the vibrating atom vibrates periodically.

In our work, the displacements of the carbon atoms in the same row of the vibrating atom were calculated. Here, we take

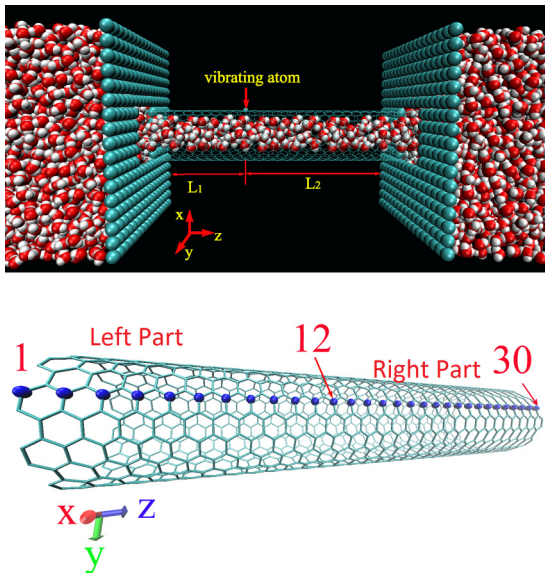


FIG. 1. (Color online) Upper panel: snapshot of the simulation system. Two reservoirs are connected by an uncapped (10,10) SWNT combined with two carbon planes. The red and white balls represent the oxygen and hydrogen atoms in water molecules, respectively. A vibrating atom of the SWNT (10,10) vibrates along the  $x$  axis periodically. Lower panel: zoomed side view of the SWNT. Carbon atoms in the same row as the vibrating atom are labeled with numbers. All molecular visualizations were generated using the VMD software package [43].

the average of these displacements according to the formula

$$x_i - x_0 = \frac{1}{N} \sum_{n=0}^{N-1} [x_i(t + nT) - x_0],$$

where  $x_0$  is the initial  $x$  coordinate of the 12th carbon atom, which is the vibrating atom,  $x_i(t + nT)$  is the  $x$  coordinate of the  $i$ th carbon atom in the same row as the vibrating atom at  $t = t + nT$ ,  $T$  is the vibration period of the 12th carbon atom, and the total simulation time is  $NT$ . The size of the vibration region is twice the vibration amplitude of the carbon atom.

For sys1, the 12th carbon atom, which is located 9 Å from the center of the CNT, is chosen as the vibrating atom (see Fig. 1). The distance from the vibrating atom to the left end of the CNT,  $L_1$ , is 37% of the total length of the CNT. The amplitude of the vibration  $A$  is 0.15 nm. A series of simulations were carried out for vibration frequencies between 10 and 5000 GHz. With a further increase in the vibration frequency, the SWNT is broken by the mechanical vibration. The time for each simulation was 105 ns, and simulation data for the last 100 ns were collected for analysis.

The second system, named sys2, contains a (6,6) SWNT with length of 7.15 nm and diameter of 0.81 nm; i.e., the length of the SWNT is the same as that of the (10,10) SWNT in sys1. To ensure the same ratio  $L_1/L$ , the 12th carbon atom is again chosen as the vibrating atom. The vibration amplitude is 0.075 nm.

The third system, named sys3, contains a (10,10) SWNT with length of 14.43 nm. To ensure a similar ratio  $L_1/L$ , the 23rd carbon atom is chosen as the vibrating atom considering that the SWNT in sys3 is about twice as long as that in sys1.

A leapfrog algorithm for integrating Newton's equations of motion was chosen in our simulations. The time step for integration was 1 fs. All molecular dynamics simulations were carried out for a constant particle number, volume (box dimensions for sys1 and sys2 were  $L_x = 5.0$  nm,  $L_y = 5.0$  nm, and  $L_z = 14.0$  nm while box dimensions for sys3 were  $L_x = 5.0$  nm,  $L_y = 5.0$  nm, and  $L_z = 21.0$  nm) and temperature (300 K) using GROMACS 4.0.7 [44]. A dynamics process was carried out to allow the system to exchange heat, which was controlled using a V-rescale thermostat with  $\tau = 0.1$  ps [45]. This thermostat functions similarly to Berendsen coupling, but the stochastic term ensures that a proper canonical ensemble is generated. Periodic boundary conditions were applied in all directions. Here water was modeled using the transferable intermolecular potential 3 points (TIP3P) model. The CNT is regarded as a whole molecule comprising many carbon atoms that in turn can be regarded as material points. The Lennard-Jones parameters for the interaction among carbon atoms were a cross section of  $\sigma_{CC} = 0.34$  nm, a depth of the potential well  $\epsilon_{CC} = 0.3612$  kJ mol $^{-1}$ , carbon-carbon bond lengths of  $r_0 = 0.142$  nm, bond angles of  $\theta_0 = 120^\circ$ , and spring constants  $k_b = 393\,960$  kJ mol $^{-1}$  nm $^{-2}$ ,  $k_\theta = 527$  kJ mol $^{-1}$  deg $^{-2}$ , and  $k_\xi = 52.718$  kJ mol $^{-1}$  deg $^{-2}$ . The water-carbon interaction was a van der Waals interaction with cross section  $\sigma_{CO} = 0.3275$  nm and  $\epsilon_{CO} = 0.4802$  kJ mol $^{-1}$ . All parameters were taken from the work of Hummer *et al.* [8]. The long-range Coulombic interactions were handled using the particle mesh Ewald (PME) method with a cutoff of 1.4 nm, fast Fourier transform (FFT) grid spacing of 0.12 nm, and fourth-order interpolation.

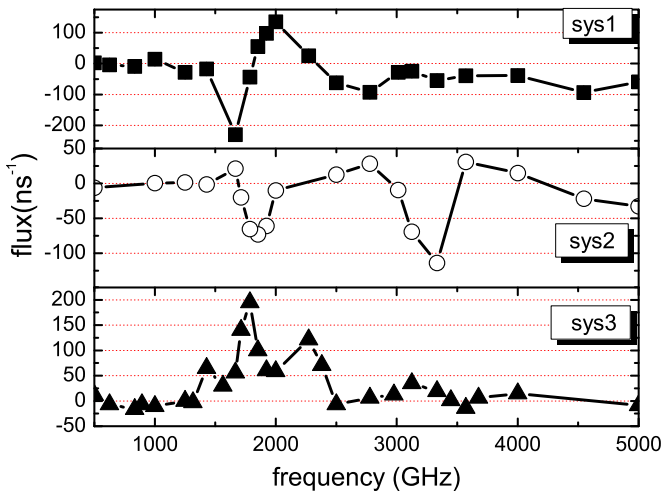


FIG. 2. (Color online) Average water flux as a function of the vibration frequency.

The short-range van der Waals forces were calculated by applying a cutoff scheme with a cutoff distance of 1.4 nm.

### III. RESULTS AND DISCUSSION

Figure 2 shows the water flux as a function of the vibration frequency for different systems. The water flux can be calculated as  $\text{flux} = [N_{\text{right}}(t) - N_{\text{left}}(t)]/t$ , where  $N_{\text{right}}(t)$  is the number of water molecules that have crossed the CNT from the left end to the right end during time  $t$  and  $N_{\text{left}}(t)$  is the number of water molecules that have crossed the CNT from the right end to the left end during time  $t$  (the last 100 ns). It is clear that the water flux is almost zero in the low-frequency range ( $<1000$  GHz). However, it is sensitive to the vibration frequency in the range of 1000 to 5000 GHz, which corresponds to the resonance frequency of water inside the SWNT [41,46]. The vibration frequency is within the working range of the self-breathing frequency of the SWNT or current terahertz technology [47]. For sys1, there are two main peaks in the flux curve. One is negative at  $f_1 = 1666.7$  GHz and the other is positive at  $f_2 = 2000$  GHz. To our surprise, the water flux undergoes sign reversal when the vibration frequency increases from  $f_1$  to  $f_2$ , indicating that the direction of water flux is not merely dependent on the asymmetry of the nanoscale system. The frequency of the external stimulus also plays a key role in water transport through the SWNT.

For sys2, water molecules confined inside a (6,6) SWNT form a single-file chain, very different from the structure of water molecules confined in the (10,10) SWNT. There are two negative peak values at 1851.9 and 3333.3 GHz. The region of the resonance frequency is consistent with the results of previous work [41]. However, the water transportation behavior is very different owing to the different vibration method employed.

For sys3, there are positive peaks in the frequency range from about 1500 to 2500 GHz, and the two main peak values around 1785.7 and 2272.7 GHz are 195 and 121  $\text{ns}^{-1}$ , respectively. In this region, the water flux does not undergo sign reversal as in the case of sys1, indicating that the relationship between the water flux and vibration frequency also depends

on the length of the SWNT. However, the resonance regions of sys1 and sys3 are similar.

Our simulation results indicate that the relationship between the water flux and the vibration frequency is complicated. It is difficult to understand the relationship and predict the actual direction of the water transport from the theory of fluid flow. In fact, this remains an unanswered question for macroscopic valveless pumps. Further theoretical work is needed to ascertain the relationship between the water flux through the SWNT and the vibration frequency of the external stimulus.

To investigate the mechanism of pumping water and what causes current reversals, we analyzed the mechanical wave propagation in the SWNT and the motions of the carbon atoms in line with the vibrating carbon atom for typical vibration frequencies of  $f = 500, 1666.7$ , and 2000 GHz. The results are shown in Fig. 3. Similarly to bowing a violin, the forced oscillation of the 12th carbon atom creates a mechanical disturbance, which moves from the position of the 12th carbon atom toward the two ends of the CNT. For the low frequency  $f = 500$  GHz [Fig. 3(a)], the motions of the carbon atoms are almost in phase. The mechanical waves do not seem to move owing to reflections of waves from the ends of the SWNT; i.e., the waves are standing waves [Figs. 3(a) and 3(b)]. However, the vibration amplitude decays with distance sharply as shown in Fig. 3(g). This decay is due to the nonconservative damping force removing energy from the system and the vibration frequency of the stimulus being far from the resonance frequency of the SWNT. The mechanical wave propagation in the SWNT is complicated by reflections and dissipation. The wave velocity is dependent on the vibration frequency [48,49]. Here, we pay particular attention to the relationship between the characteristics of mechanical wave propagation in the SWNT and the water transport through the SWNT.

It is observed that the phase difference between two waves propagating to the two ends of the SWNT has been produced under  $f = 1666.7$  GHz. According to Figs. 3(c) and 3(d), the phase speed of the wave propagating to the right end of the SWNT (positive  $z$ ) is higher than that of the wave propagating to the left end of the SWNT (negative  $z$ ). Furthermore, it is seen from Fig. 3(g) that the vibration amplitudes of the left carbon atoms (label numbers less than 12) are larger than those of the right carbon atoms (label numbers greater than 12), resulting in negative water flux through the SWNT.

In the case of  $f = 2000$  GHz [Figs. 3(e) and 3(f)], a phase difference between the two waves propagating in the SWNT is again observed. Different from the results for  $f = 1666.7$  GHz, the phase speed of the wave propagating to the right end of the SWNT is lower than that of the wave propagating to the left end of the SWNT. The wave propagating to the right decays more slowly than that propagating to the left [see Fig. 3(g)], resulting in positive water flux. All these results indicate that the value and direction of the average water flux are mainly controlled by differences in the phase and decay between the two waves propagating toward the two ends of the SWNT.

In sys2, the (6,6) SWNT has the same length as the (10,10) SWNT in sys1, but the water transport behaviors of the two SWNTs are very different. There are two negative peaks in the flux curve of sys2 (see Fig. 2). What causes the

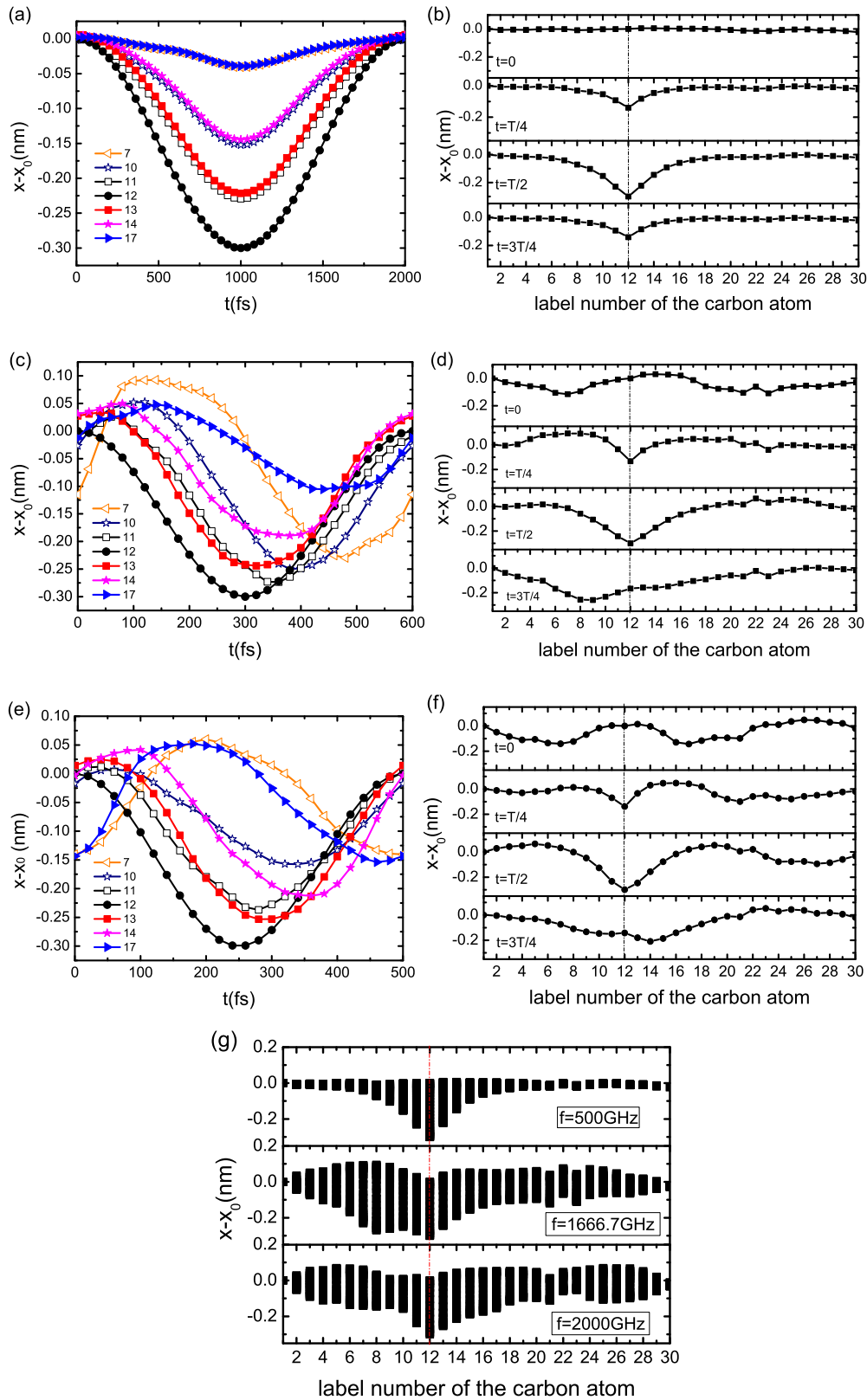


FIG. 3. (Color online) Oscillatory motion and wave propagation in the (10,10) SWNT for sys1. (a), (c), (e) Displacement  $x - x_0$  versus time for the 7th, 10th, 11th, 12th, 13th, 14th, and 17th carbon atoms in one period under  $f = 500$  GHz (a),  $f = 1666.7$  GHz (c),  $f = 2000$  GHz (e).  $x_0$  is the initial  $x$  coordinate of the 12th carbon atom, which is the forced-vibration atom. (b), (d), (f): Wave propagation in the SWNT generated by mechanical vibration of the 12th carbon atom under  $f = 500$  GHz (b),  $f = 1666.7$  GHz (d),  $f = 2000$  GHz (f).  $T$  is the period. (g): Black bars denote the vibration regions of the carbon atoms in the same top row as the vibrating atom. The height of the bar is twice the vibration amplitude of the carbon atom.

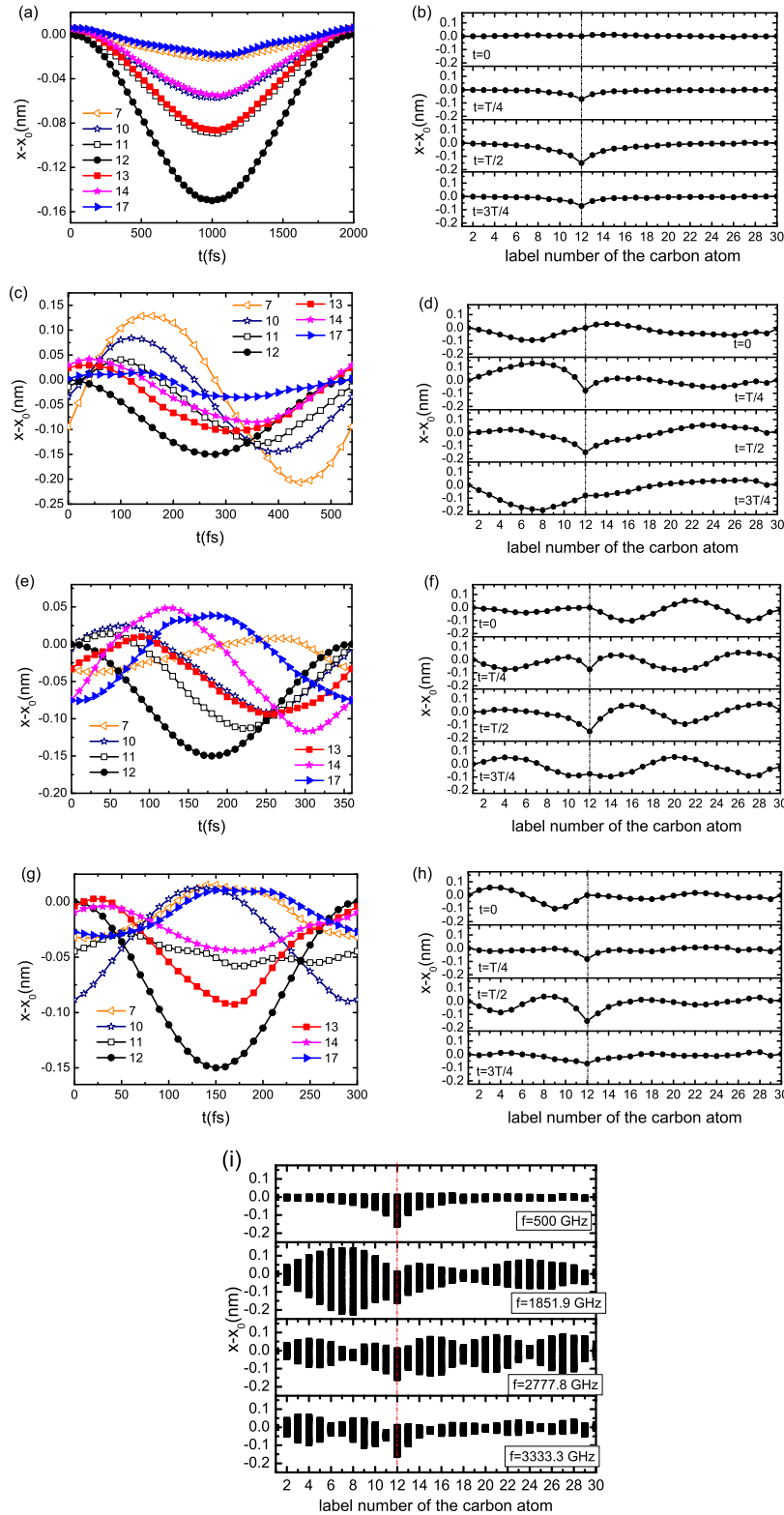


FIG. 4. (Color online) Oscillatory motion and wave propagation for sys2. (a), (c), (e), (g) Displacement  $x - x_0$  versus time for the 7th, 10th, 11th, 12th, 13th, 14th, and 17th carbon atoms in one period under  $f = 500$  GHz (a),  $f = 1851.9$  GHz (c),  $f = 2777.8$  GHz (e),  $f = 3333.3$  GHz (g).  $x_0$  is the initial  $x$  coordinate of the 12th carbon atom, which is the vibrating atom. (b), (d), (f), (h) Wave propagation in the SWNT generated by mechanical vibration of the 12th carbon atom under  $f = 500$  GHz (b),  $f = 1851.9$  GHz (d),  $f = 2777.8$  GHz (f),  $f = 3333.3$  GHz (h).  $T$  is the period. (i): Black bars denote the vibration regions of the carbon atoms in the same top row as the vibrating atom. The height of the bar is twice the vibration amplitude of the carbon atom.

difference in the water transport behavior? Here, we analyze the wave propagation for typical vibration frequencies of  $f = 500$  GHz (flux =  $-6 \text{ ns}^{-1}$ ),  $1851.9$  GHz (flux =  $-73 \text{ ns}^{-1}$ , the first negative peak),  $2777.8$  GHz (flux =  $28 \text{ ns}^{-1}$ ), and  $3333.3$  GHz (flux =  $-114 \text{ ns}^{-1}$ , the second negative peak).

In the case of  $f = 500$  GHz, the motions of carbon atoms in sys2 are similar to those of the carbon atoms in sys1. The carbon atoms in the two systems have the same phases [Figs. 4(a) and 4(b)]. Furthermore, it is seen from Fig. 4(i) that the amplitude decreases dramatically with the distance owing to the nonconservative damping force, indicating that not all external vibrations lead to steady-state wave propagations. When the difference in vibration amplitudes of the carbon atoms located on the two sides of the forced-vibration atom is slight, the flux is low.

For  $f = 1851.9$  GHz [Figs. 4(c) and 4(d)], the differences in the phase and decay between two waves propagating toward the two ends of the SWNT are obvious. The simulation result is very similar to the result for sys1 at  $f = 1666.7$  GHz. The speed of the mechanical wave propagating to the right end of the SWNT is higher than that of the mechanical wave propagating to the left end. The vibration amplitudes of the left carbon atoms are larger than those of the right carbon atoms, resulting in the flux entering a trough (the first negative peak) at  $f = 1851.9$  GHz.

In the case of  $f = 2777.8$  GHz [Figs. 4(e) and 4(f)], in contrast to the results for  $f = 1851.9$  GHz, the speed of the wave propagating to the right end of the SWNT is lower than that of the wave propagating to the left end. As shown in Fig. 4(i), the vibration amplitudes of the right carbon atoms are larger than those of the left carbon atoms, resulting in positive water flux.

However, when the vibration frequency is  $3333.3$  GHz, the direction of flux reverses again. Different from the results for  $f = 2777.8$  GHz, the speed of the wave propagating to the right end is higher than that of the wave propagating to the left end. The vibration amplitude of the carbon atoms on the left is larger than that of the carbon atoms on the right.

The flux of sys3 is very different from that of sys1, but the mechanism of pumping water is the same. Figure 5 shows the oscillatory motion, wave propagation, and vibration amplitude for typical frequencies of  $f = 500$  and  $1785.7$  GHz. In the case of  $f = 500$  GHz, we see from Figs. 5(a) and 5(b) that a quasi-steady-state standing wave is generated successfully in the SWNT. The mechanical energy is pumped into the system continuously by the 23rd carbon atom (the forced-vibration atom). It is apparent from Fig. 5(e) that the vibration amplitude is larger than that of sys1 at  $f = 500$  GHz. However, the corresponding flux is very low (about  $11 \text{ ns}^{-1}$ ) because the vibration frequency is not in the region of the resonance frequency of water. When the vibration frequency increases to  $1785.7$  GHz, the hydrogen bonds between water molecules inside the SWNT are broken by the resonance. Therefore, the motions of water molecules confined in the SWNT are very rapid. The vibration amplitudes of the right carbon atoms are larger than those of the left carbon atoms. Hence, the flux reaches a positive peak ( $195 \text{ ns}^{-1}$ ).

The three systems have analogs for the relationship between the flux and the characteristics of mechanical wave propagation. The above discussions reveal the conditions required

to produce the rapid directed transport of water molecules through the SWNT. First, the vibration frequency of the external stimulus is in the resonance region of water molecules. Second, there is an obvious vibration amplitude difference between the two parts of the SWNT. When the vibration amplitude of the left part of the SWNT is larger than that of the right part, it is easier for water molecules to move from right to left than from left to right, and vice versa.

We also calculated the water density distributions along the  $z$  axis inside the CNT; results are shown in Fig. 6. It is seen that the profile of water density along the  $z$  axis forms a valley in the region (see the dashed line in Fig. 6) where the vibrating atom is located. For sys1, it is seen from Fig. 6(a) that the water density, especially that at the location of the vibrating atom, decreases as the vibration frequency approaches  $f_1 = 1666.7$  GHz. For  $1666.7 \text{ GHz} \leq f \leq 5000 \text{ GHz}$ , the profile of the water density in the valley changes slightly but very importantly; this is related to the direction of water flux. For easy discussion, we separate the CNT into two parts from the position of the vibrating atom (denoted by the dashed line in Fig. 6): the left part and the right part. It is interesting that the gradients of the right and left parts of the density curve close to the vibrating atom are very different. For  $f = 1666.7$  GHz (correspondingly, flux =  $-230 \text{ ns}^{-1}$ ), the gradient of the right part of the water density curve is greater than that of the left part, revealing that the pressure gradient of the right part is greater than that of the left part. The direction of the water current is therefore negative. For  $f = 2000$  GHz (correspondingly flux =  $135 \text{ ns}^{-1}$ ), in contrast, the gradient of the water density curve in the left region is greater than that in the right region.

For sys2, a wavelike pattern of the water density distribution is observed, because the water molecules form a single-file water chain inside the (6,6) SWNT. The mechanism behind this phenomenon was investigated in our previous paper [50]. As in sys1, the water density decreases as the vibration frequency increases. When the vibration frequency increases to  $f = 1851.9$  GHz, the water density at the location of the vibrating atom decreases dramatically owing to the resonant response of the water chain to the vibration of the CNT. This is consistent with the results of previous works [41,46]. Correspondingly, the water flux reaches a negative peak (flux =  $-73 \text{ ns}^{-1}$ ). The density in the left part is lower than that in the right part, because the vibration amplitudes of carbon atoms in the left part are larger than those in the right part. In the case of  $f = 2777.7$  GHz, the direction of the water current is positive, in contrast to that in the case of  $f = 1851.9$  GHz. The water density distributions are very different for these two frequencies. According to Fig. 6(b), the water density in the right part decreases dramatically owing to the sharp increase in the vibration amplitudes of the carbon atoms in the right part [see Fig. 4(i)].

For sys3, the profile of the water density distribution along the nanotube axis is similar to that for sys1. However, the water density at the position close to the right end of the SWNT is higher than that for sys1. This is because the SWNT in sys3 is longer than that in sys1 and the amplitude of the mechanical wave propagating in the SWNT decays with distance. The vibration amplitude of the carbon atoms close to the right end of the SWNT in sys3 is smaller than that in sys1.

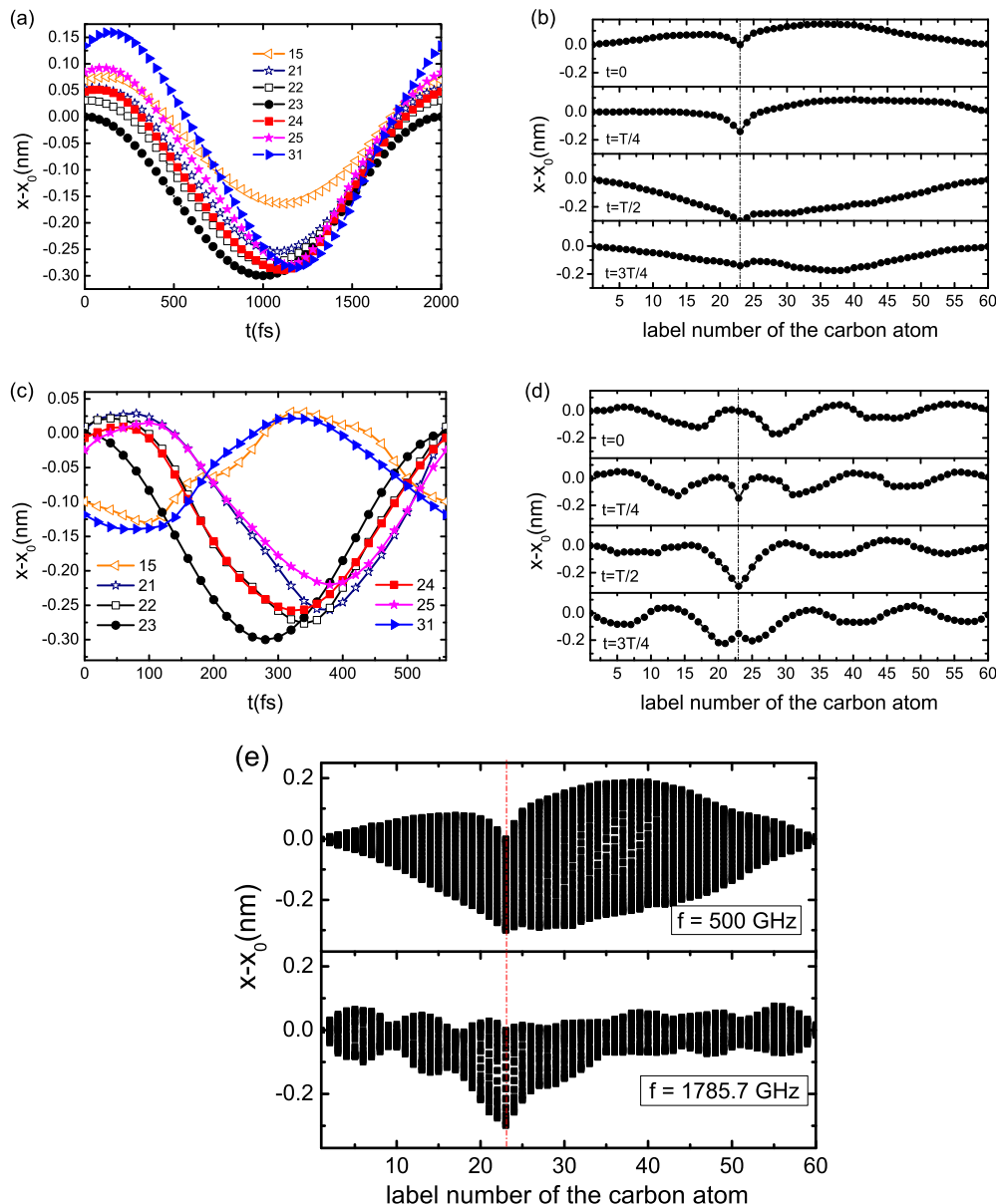


FIG. 5. (Color online) Oscillatory motion and wave propagation for sys3. (a),(c) Displacement  $x - x_0$  versus time for the 15th, 21st, 22nd, 23rd, 24th, 25th, and 31st carbon atoms in one period under  $f = 500$  GHz (a),  $f = 1785.7$  GHz (c).  $x_0$  is the initial  $x$  coordinate of the 23rd carbon atom, which is the vibrating atom. (b), (d) Wave generated by mechanical vibration of the 23rd carbon atom under  $f = 500$  GHz (b),  $f = 1785.7$  GHz (d).  $T$  is the period. (e): Black bars denote the vibration regions of the carbon atoms in the same top row as the vibrating atom. The height of the bar is twice the vibration amplitude of the carbon atom.

We note that the direction of the water flux depends on the difference between the right and left parts of the density curve in the valley. If the water density for the left region is higher (lower) than that of the right region, the water flux is positive (negative). In fact, the difference in water density between the two parts along the SWNT results from the differences in phase and decay between the two waves propagating towards the two ends. The greater the vibration amplitudes of the carbon atoms, the lower the density of water becomes under the same vibration frequency.

Hydrogen bonds play a key role in water dynamics, especially at a nanoscale. We therefore further calculated the average number of hydrogen bonds and water molecules inside

the left part and right part of the nanotube under a wide range of vibration frequencies. Here, we define  $\xi = N_{\text{HB}}/N$ , where  $N_{\text{HB}}$  is the average number of hydrogen bonds between water molecules inside the left part or right part of the SWNT, and  $N$  is the average number of water molecules inside the left part or right part of the SWNT.  $\xi_0$  is for the unperturbed system ( $f = 0$  GHz). Results are presented in Fig. 7. For sys1 [Fig. 7(a)], we observe that the number of hydrogen bonds decreases sharply to a minimum at a frequency of 1666.7 GHz for the water molecules in the left part and at a frequency of 2000 GHz for the water molecules in the right part. In the case of  $f = 1666.7$  GHz, each water molecule in the left part has about 0.3 hydrogen bonds, only 29.4% of the number for the

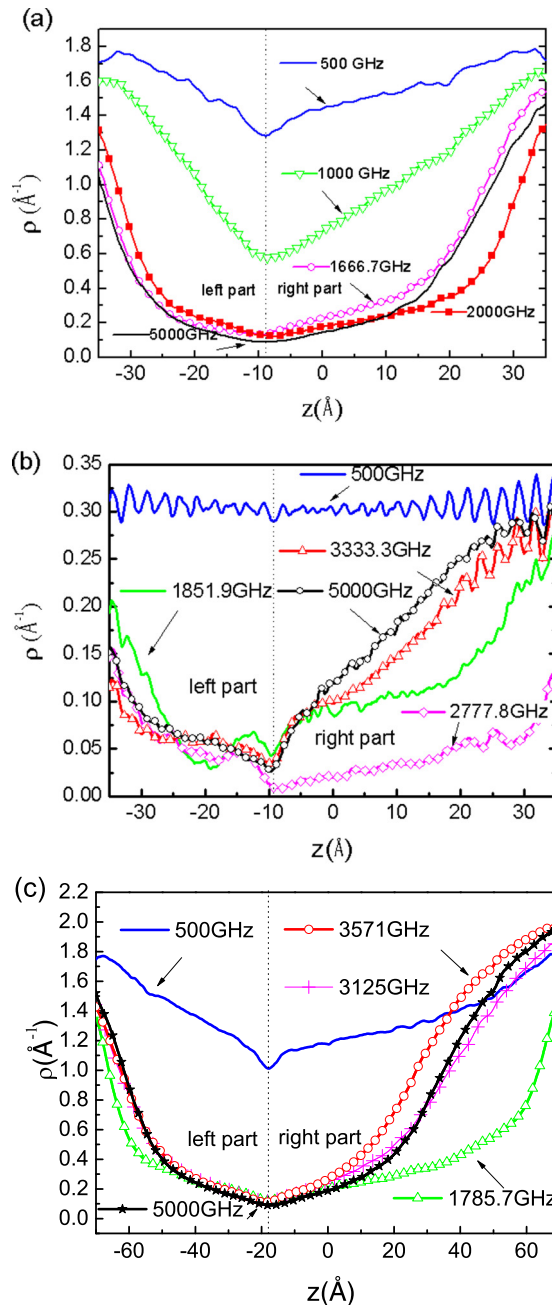


FIG. 6. (Color online) Water distribution along the nanotube axis for sys1 (a), sys2 (b), and sys3 (c).

unperturbed system. However, each water molecule in the right part has about 0.5 hydrogen bonds, 49.1% of the number for the unperturbed system. In the case of  $f = 2000$  GHz, each water molecule in the right part has about 0.33 hydrogen bonds and each water molecule in the left part has about 0.38 hydrogen bonds. These numbers correspond to 32.9% and 38.1% of the numbers for the unperturbed system, respectively.

For sys2, there are peaks in the ratio curves of the hydrogen bond number [Fig. 7(b)] at the vibration frequencies  $f = 1851.9$  GHz and  $f = 3333.3$  GHz. The two main peak values of water flux around 1851.9 and 3333.3 GHz are  $-73$  and  $-114 \text{ ns}^{-1}$ , respectively. The ratio  $\xi$  of the average number of hydrogen bonds between water molecules in the left part of

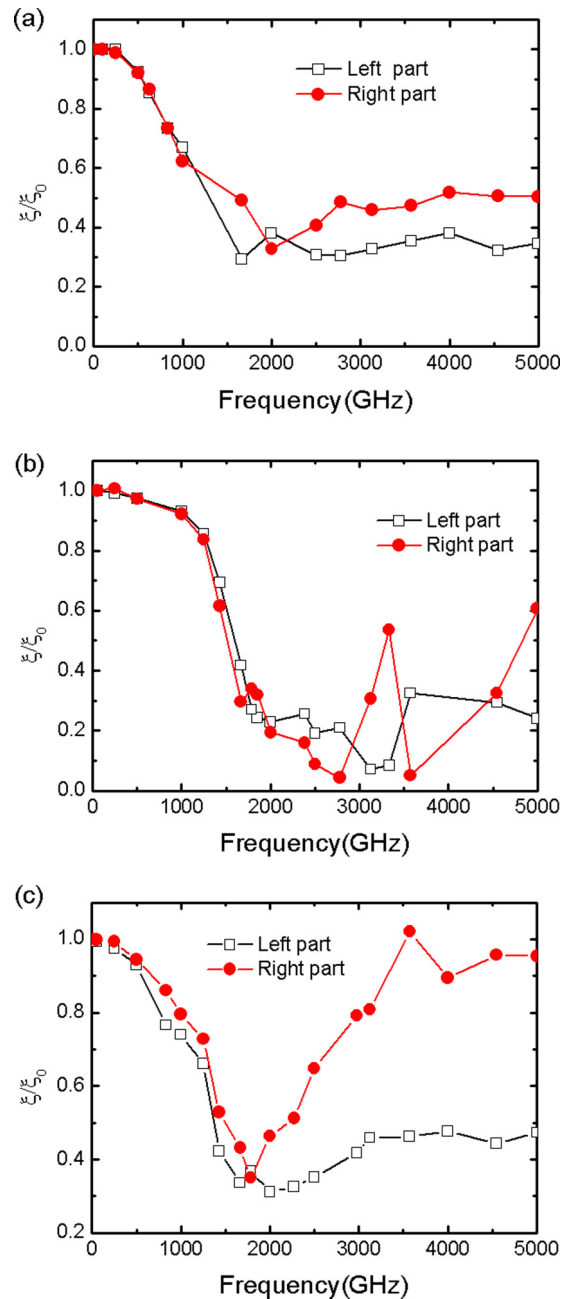


FIG. 7. (Color online) Hydrogen bonds between water molecules inside the CNT for different frequencies.  $\xi$  is the average number of hydrogen bonds per water molecule for the left part or right part of the SWNT. (a), (b), and (c) are results for sys1, sys2, and sys3, respectively.

the SWNT reaches a negative trough and  $\xi$  of the right part peaks. Comparing with Fig. 6(b), we see that the number of hydrogen bonds varies with the density of water molecules in the SWNT. As the water density decreases, the probability of hydrogen bond formation decreases.

For sys3, the number of hydrogen bonds in the right part is different from that in sys1 and sys2 when the vibration frequency exceeds 1785.7 GHz. The number of hydrogen bonds between water molecules in the right part of the SWNT increases with the vibration frequency of the external

stimulus in the range of  $f > 1785.7$  GHz. This is because the vibration amplitudes of the carbon atoms close to the right end of the SWNT are smaller than those for sys1 and sys2. Correspondingly, the water density in the right part is higher than that in the left part.

As the vibration frequency approaches the resonance frequency of water molecules inside the SWNT, the water density at the position of the vibration atom decreases dramatically. Additionally, the number of hydrogen bonds connecting with water molecules inside the SWNT decreases sharply. When the vibration amplitude of carbon atoms in the left part is larger (smaller) than that of carbon atoms in the right part, the water density in the left part is lower (higher) than that in the right part. Correspondingly, the number of hydrogen bonds connecting with water molecules in the left part is smaller (greater) than that of hydrogen bonds connecting with water molecules in the right part. The direction of water flux is thus negative (positive).

The resonance frequency of water molecules inside the SWNT is consistent with the results of previous Raman spectral experiments and simulations. Experimental results showed multiple Raman spectral peaks for bulk water or water confined inside a nanotube. These peaks are attributed to O-H bond relaxation, O-H rotation relaxation, O-H warp relaxation, and so forth [12,51].

We also conducted simulations to investigate effects of the position of the forced vibrating atom on the transport of water through the SWNT. The flux is sensitive to the position of the vibrating atom. However, the mechanism is the same.

In this study, a V-rescale thermostat was chosen for temperature coupling with  $\tau = 0.1$  ps. In addition, we checked our simulation results at  $f = 1666.7$  GHz by choosing different time scales of operation ( $\tau = 0.1, 0.08,$  and  $0.05$  ps). Here, the time for each simulation is 60 ns. The water flux fluctuates within a reasonable region:  $\tau = 0.1$  ps, flux =  $-230 \text{ ns}^{-1}$ ;  $\tau = 0.08$  ps, flux =  $-227 \text{ ns}^{-1}$ ;  $\tau = 0.05$  ps, flux =  $-243 \text{ ns}^{-1}$ . Furthermore, we checked our simulation results by changing the size of the water reservoir. From our simulation results, we found that the water flux is mainly controlled by the mechanical waves propagating in the CNT and the resonant region of water molecules in the CNT. The mechanical waves depend on mechanical properties of the CNT and the resonant region of water molecules mainly depends on the hydrogen

bonds connecting the water molecules. Neither is sensitive to temperature coupling.

#### IV. CONCLUSIONS

In summary, we proposed a valveless nanosized pump and found current inversions in this nanoscale fluidic system. It was found that current inversion is induced by the inversions of the differences in the phase and decay between the two waves generated by mechanical vibrating and propagating toward the two ends of the CNT. The differences in phase and decay between the two waves depend on the vibration frequency, and induce differences in the water density and hydrogen bonds for two regions (left and right parts) of the CNT. Furthermore, we found the conditions required to produce rapid directed transport of water through the SWNT driven by mechanical vibration. The first factor is that the frequency of mechanical vibration is in the resonance region of water molecules confined in the SWNT. The second factor is that there is an obvious difference in vibration amplitude between the two parts of the SWNT. When the vibration amplitudes of the carbon atoms in the left part are larger than those of the carbon atoms in the right part, it is easier for water molecules to move from right to left than from left to right, and vice versa. Our simulation results reveal that the transport of water molecules can be driven by mechanical wave propagation in the CNT. In an experiment, mechanical wave propagation in a CNT can be generated and sustained by oscillating tips, such as the tips of an atomic force microscope or cantilever-mounted tips. This work thus revealed an additional mechanism of current inversions in the nanosized water pump, which may find application in the design of nanofluidic systems.

#### ACKNOWLEDGMENTS

This work is partially supported by the National Natural Science Foundation of China (Grants No. 11505156, No. 11405146, and No. 61274099), the China Scholarship Council (Grant No. 201308330031), the Zhejiang Provincial Science and Technology Key Innovation Team (Grant No. 2011R50012), and the Zhejiang Provincial Key Laboratory (Grant No. 2013E10022).

- 
- [1] M. Majumder, N. Chopra, R. Andrews, and B. J. Hinds, *Nature (London)* **438**, 930 (2005).
  - [2] K. Koga, G. T. Gao, H. Tanaka, and X. C. Zeng, *Nature (London)* **412**, 802 (2001).
  - [3] M. Whitby and N. Quirke, *Nat. Nanotechnol.* **2**, 87 (2007).
  - [4] A. Kalra, S. Garde, and G. Hummer, *Proc. Natl. Acad. Sci. USA* **100**, 10175 (2003).
  - [5] A. Noy, H. G. Park, F. Fornasiero, J. K. Holt, C. P. Grigoropoulos, and O. Bakajin, *Nano Today* **2**, 22 (2007).
  - [6] A. Bianco, K. Kostarelos, and M. Prato, *Curr. Opin. Chem. Biol.* **9**, 674 (2005).
  - [7] H. G. Park and Y. Jung, *Chem. Soc. Rev.* **43**, 565 (2014).
  - [8] G. Hummer, J. C. Rasaiah, and J. P. Noworyta, *Nature (London)* **414**, 188 (2001).
  - [9] N. Naguib, H. H. Ye, Y. Gogotsi, A. G. Yazicioglu, C. M. Megaridis, and M. Yoshimura, *Nano Lett.* **4**, 2237 (2004).
  - [10] K. Koga, H. Tanaka, and X. Zeng, *Nature (London)* **408**, 564 (2000).
  - [11] S. Joseph and N. R. Aluru, *Nano Lett.* **8**, 452 (2008).
  - [12] H. D. Lee, H. W. Kim, Y. H. Cho, and H. B. Park, *Small* **10**, 2653 (2014).
  - [13] Y. Zhao *et al.*, *Adv. Mater.* **20**, 1772 (2008).
  - [14] Q. Yuan and Y.-P. Zhao, *J. Am. Chem. Soc.* **131**, 6374 (2009).
  - [15] S. Ghosh, A. K. Sood, and N. Kumar, *Science* **299**, 1042 (2003).

- [16] P. Král and M. Shapiro, *Phys. Rev. Lett.* **86**, 131 (2001).
- [17] J.-w. Feng, H.-m. Ding, C.-l. Ren, and Y.-q. Ma, *Nanoscale* **6**, 13606 (2014).
- [18] X.-P. Li, G.-P. Kong, X. Zhang, and G.-W. He, *Appl. Phys. Lett.* **103**, 143117 (2013).
- [19] S. De Luca, B. Todd, J. Hansen, and P. J. Daivis, *J. Chem. Phys.* **138**, 154712 (2013).
- [20] K. F. Rinne, S. Gekle, D. J. Bonthuis, and R. R. Netz, *Nano Lett.* **12**, 1780 (2012).
- [21] Y. Wang, Y. J. Zhao, and J. P. Huang, *J. Phys. Chem. B* **115**, 13275 (2011).
- [22] M. Longhurst and N. Quirke, *Nano Lett.* **7**, 3324 (2007).
- [23] Z. Insepov, D. Wolf, and A. Hassanein, *Nano Lett.* **6**, 1893 (2006).
- [24] B. Wang and P. Král, *J. Am. Chem. Soc.* **128**, 15984 (2006).
- [25] S. De Luca, B. D. Todd, J. S. Hansen, and P. J. Daivis, *Langmuir* **30**, 3095 (2014).
- [26] P. Král and D. Tománek, *Phys. Rev. Lett.* **82**, 5373 (1999).
- [27] W. H. Duan and Q. Wang, *ACS Nano* **4**, 2338 (2010).
- [28] H. A. Zambrano, J. H. Walther, P. Koumoutsakos, and I. F. Sbalzarini, *Nano Lett.* **9**, 66 (2008).
- [29] J. Zheng, E. M. Lennon, H. K. Tsao, Y. J. Sheng, and S. Jiang, *J. Chem. Phys.* **122**, 214702 (2005).
- [30] Z.-Q. Zhang, X. Dong, H.-F. Ye, G.-G. Cheng, J.-N. Ding, and Z.-Y. Ling, *J. Appl. Phys.* **116**, 074307 (2014).
- [31] J. Zhao, J.-Q. Huang, F. Wei, and J. Zhu, *Nano Lett.* **10**, 4309 (2010).
- [32] A. B. D. Brown, C. G. Smith, and A. R. Rennie, *Phys. Rev. E* **63**, 016305 (2000).
- [33] X. Zhou, F. Wu, J. Kou, X. Nie, Y. Liu, and H. Lu, *J. Phys. Chem. B* **117**, 11681 (2013).
- [34] H. Lu, X. Nie, F. Wu, X. Zhou, and J. Kou, *J. Chem. Phys.* **136**, 174511 (2012).
- [35] X. Zhou, J. Kou, X. Nie, F. Wu, Y. Liu, and H. Lu, *Chin. Phys. B* **24**, 074702 (2015).
- [36] B. Wang and P. Král, *Phys. Rev. Lett.* **98**, 266102 (2007).
- [37] T. Chang, *Phys. Rev. Lett.* **101**, 175501 (2008).
- [38] H. Qiu, R. Shen, and W. Guo, *Nano Res.* **4**, 284 (2011).
- [39] J. Kou, X. Zhou, H. Lu, Y. Xu, F. Wu, and J. Fan, *Soft Matter* **8**, 12111 (2012).
- [40] J. Kou, H. Lu, F. Wu, J. Fan, and J. Yao, *Nano Lett.* **14**, 4931 (2014).
- [41] Q.-L. Zhang, W.-Z. Jiang, J. Liu, R.-D. Miao, and N. Sheng, *Phys. Rev. Lett.* **110**, 254501 (2013).
- [42] P. Reimann, *Phys. Rep.* **361**, 57 (2002).
- [43] W. Humphrey, A. Dalke, and K. Schulten, *J. Mol. Graphics* **14**, 33 (1996).
- [44] H. J. C. Berendsen, D. Vandespoel, and R. Vandrungen, *Comput. Phys. Commun.* **91**, 43 (1995).
- [45] G. Bussi, D. Donadio, and M. Parrinello, *J. Chem. Phys.* **126**, 014101 (2007).
- [46] H. J. Lu, X. J. Gong, C. L. Wang, H. P. Fang, and R. Z. Wang, *Chin. Phys. Lett.* **25**, 1145 (2008).
- [47] H. M. Lawler, D. Areshkin, J. W. Mintmire, and C. T. White, *Phys. Rev. B* **72**, 233403 (2005).
- [48] M. Chen, J. Zang, D. Xiao, and F. Liu, *J. Appl. Phys.* **105**, 026102 (2009).
- [49] V. N. Popov, V. E. Van Doren, and M. Balkanski, *Phys. Rev. B* **61**, 3078 (2000).
- [50] H. Lu, J. Li, X. Gong, R. Wan, L. Zeng, and H. Fang, *Phys. Rev. B* **77**, 174115 (2008).
- [51] S. Cambré, B. Schoeters, S. Luyckx, E. Goovaerts, and W. Wenseleers, *Phys. Rev. Lett.* **104**, 207401 (2010).